

Comment: This manuscript is an initial-submission version of “Photonuclear Reactions Triggered by Lightning Discharge” which was accepted for publication in the 23 November 2017 issue of Nature as a Letter (DOI 10.1038/nature24630). This manuscript has not undergone the peer review process. See the accepted version at the Nature website: <http://dx.doi.org/10.1038/nature24630>

arXiv:1711.08044v1 [astro-ph.HE] 21 Nov 2017

Photonuclear Reactions in Lightning Discovered from Detection of Positrons and Neutrons

Teruaki Enoto^{1*}, Yuuki Wada^{2,3}, Yoshihiro Furuta², Kazuhiro Nakazawa^{2,4}, Takayuki Yuasa⁵, Kazufumi Okuda², Kazuo Makishima⁶, Mitsuteru Sato⁷, Yousuke Sato⁸, Toshio Nakano³, Daigo Umemoto⁹ & Harufumi Tsuchiya¹⁰

¹*The Hakubi Center for Advanced Research and Department of Astronomy, Kyoto University, Kyoto 606-8302, Japan*

²*Department of Physics, Graduate School of Science, The University of Tokyo, Tokyo 113-0033, Japan*

³*High Energy Astrophysics Laboratory, RIKEN Nishina Center, Saitama 351-0198, Japan*

⁴*Research Center for the Early Universe, The University of Tokyo, Tokyo 113-0033, Japan*

⁵*55 Devonshire Road 239855, Singapore*

⁶*MAXI Team, The Institute of Physics and Chemical Research (RIKEN), Saitama 351-0198, Japan*

⁷*Graduate School of Science, Hokkaido University, Sapporo 060-0808, Japan*

⁸*Department of Applied Energy, Graduate School of Engineering, Nagoya University, Aichi 464-8603, Japan*

⁹*Advanced Institute for Computational Science, RIKEN, Hyogo 650-0047, Japan*

¹⁰*Nuclear Science and Engineering Center, Japan Atomic Energy Agency, Ibaraki 319-1195, Japan*

Lightning and thundercloud are the most dramatic natural particle accelerators on the Earth ¹. Relativistic electrons accelerated by electric fields therein emit bremsstrahlung gamma rays ^{2,3}, which have been detected at ground observations ⁴⁻⁹, by airborne detectors ¹⁰⁻¹², and as terrestrial gamma-ray flashes (TGFs) from space ¹³⁻¹⁵. The energy of the gamma rays is sufficiently high to potentially invoke atmospheric photonuclear reactions $^{14}\text{N}(\gamma, n)^{13}\text{N}$ ^{12,16-19}, which would produce neutrons and eventually positrons via beta-plus decay of generated unstable radioactive isotopes, especially ^{13}N . However, no clear observational evidence for the reaction has been reported to date ²⁰⁻²². Here we report the first detection of neutron and positron signals from lightning with a ground observation. During a thunderstorm on 6 February 2017 in Japan, a TGF-like intense flash (< 1 ms) was detected at our monitoring sites 0.5–1.7 km away from the lightning. The subsequent initial burst quickly subsided with an exponential decay constant of 40–60 ms, followed by a prolonged line emission at ~ 0.511 megaelectronvolt (MeV), lasting for a minute. The observed decay timescale and spectral cutoff at ~ 10 MeV of the initial emission are well explained with de-excitation gamma rays from the nuclei excited by neutron capture. The centre energy of the prolonged line emission corresponds to the electron-positron annihilation, and hence is the conclusive indication of positrons produced after the lightning. Our detection of neutrons and positrons is unequivocal evidence that natural lightning triggers photonuclear reactions. No other natural event on the Earth is known to trigger photonuclear reactions. This discovery places lightning as only the second known natural channel on the Earth after the atmospheric cosmic-ray interaction,

in which isotopes, such as ^{13}C , ^{14}C , and ^{15}N , are produced.

Winter thunderstorms along the coast of the Sea of Japan are much feared natural phenomena for the locals²³. For the same reasons, the area in winter season is ideal for observing high-energy phenomena from lightning and thunderclouds *i.e.*, (1) powerful thunderstorms are frequent, (2) cold temperature lowers the cloud-base altitude down to 0.2–0.8 km^{23,24}, which allows gamma rays from it, if emitted, to reach the ground easily. With the aim of detecting gamma rays from winter thunderclouds, we started the “GROWTH project” in 2006^{7,25,26} (see Methods “GROWTH collaboration”), which was later partly funded by crowdfunding. During the winter of 2016–2017, we operated newly installed four radiation detectors A–D at the Kashiwazaki-Kariwa nuclear power station in Niigata (Fig 1a).

On 6 February 2017, a pair of negative and positive cloud-to-ground discharges occurred at 08:34:06.0027 UTC under a winter thunderstorm (see Methods “Lightning discharges”). All the four detectors, located 0.5–1.7 km away from the place of the discharges, simultaneously recorded an intense radiation lasting for ~ 200 ms (Fig 1). The radiation monitoring stations operated by the power plant also recorded this flash (see Fig 1a and Methods “Radiation monitors”). The analogue outputs of phototube amplifier exhibited strong undershoot (or equivalent) at the beginning of the event for roughly 40, 20, 20, and 300 ms in the detectors A–D, respectively (see Methods “Initial flash”). These undershoots are an instrumental response to intensive light outputs from scintillation crystals that largely exceeded the nominal instrumental dynamic range, which was triggered by a very short (< 1 ms) and strong gamma-ray flash, resembling a downward TGF²⁷. In the following analyses, we define t as the elapsed time from the epoch of the rise of the initial radiation flash.

After the initial surge of signals and after the nominal operation status of the amplifier had been restored (see Methods “Initial flash”), all the detectors recorded a sub-second decaying radiation (Fig. 1b–d). The time profile is fitted satisfactorily by an exponential form with a decay constant of 40–60 ms. The recorded event rates with the detectors A–C above 3 MeV during the sub-second radiation are 2–3 orders of magnitude higher than the environmental background. The spectra show a power-law shape with a photon index $\Gamma \sim 0.5$ below a sharp cutoff at 7–10 MeV (Fig. 2). These time profile and spectral shape suggest that the origin is different from the bremsstrahlung gamma rays in thundercloud electric fields reported in the past^{7,25}, which showed Gaussian-like time profiles lasting for a minute and had an energy spectrum with a steeper slope $\Gamma \sim 1$ –2 and less sharp cutoff at around 20 MeV.

Following the sub-second radiation, the 0.35–0.60 MeV count rates with the detectors A and D (Fig. 3a, b) increased for up to a minute. Fig. 4 shows the energy spectra during the period of the enhancement. The most striking feature in the spectra is a prominent emission line at ~ 0.51 MeV, which is in very good agreement with the energy of 0.511 MeV for electron-positron annihilation. The centre energies of the Gaussian line profiles were determined to be 0.515 ± 0.006 (stat.) ± 0.006 (sys.) MeV and 0.501 ± 0.003 (stat.) ± 0.006 (sys.) MeV for the detectors A and D, respectively (see Methods “In-

strumental calibration”). The hypothesis that the line originates from the background is thus rejected, of which the line centre energies should be either 0.583 MeV (^{208}Tl) or 0.609 MeV (^{214}Bi). The continuum is well explained by the combination of photo-absorption and Compton scattering of ~ 0.51 MeV photons, and supports the interpretation of the annihilation line from positrons (Fig.3).

The time profile of the annihilation signal (Fig. 3) showed an exponentially decaying component with time constants of 4–10 s in both the detectors. A following delayed component was also detected albeit only in the detector A, of which the profile is fitted by a Gaussian with a peak at $t_{\text{peak}} = 34.5 \pm 1.0$ s and a width of 13.2 ± 1.0 s (1σ).

What produced these positrons and how? A potential scenario is that electron-positron pairs are produced by high-energy gamma rays in the electron acceleration process ^{2,3}. However, the lack of detection of high-energy seed gamma rays (> 3 MeV, Fig. 3a, b) rejects the scenario. In addition, the environmental electric field measured on the ground was upwards during the annihilation signal (below ~ -3 kV m⁻¹), and hence positrons should not be accumulated towards the ground, and the annihilation line should not have been enhanced. Consequently, the most natural interpretation of the present data is the photonuclear reactions ¹⁶⁻¹⁹; *i.e.*, a burst (or flash) of the lightning-triggered gamma-ray photons, which caused the initial instrumental undershoot, collided with atmospheric nuclei and initiated nuclear reactions. The atmospheric photonuclear reactions $^{14}\text{N}(\gamma, n)^{13}\text{N}$ and $^{16}\text{O}(\gamma, n)^{15}\text{O}$ generate fast neutrons with a kinetic energy of $E_0 \sim 10$ MeV and unstable radioactive isotopes, which generate positrons in beta-plus decays.

Produced fast neutrons undergo moderation and diffusion down to the epithermal energy (\sim eV) via multiple elastic scatterings with atmospheric molecules, particularly nitrogen (see Methods “Neutron propagation”). During this process, 96% of neutrons disappear via charged-particle productions $^{14}\text{N}(n, p)^{14}\text{C}$, producing quasi-stable carbon isotopes ^{14}C (a half life of 5,730 years) without emitting any strong gamma rays, while the other 4% are radiatively captured by atmospheric nitrogen or matters on the ground, including those around detectors. The nuclei that captured a neutron promptly emit multiple de-excitation gamma-ray lines, e.g., $^{14}\text{N}(n, \gamma)^{15}\text{N}$. The theoretical capture rate exponentially decays with a timescale of 56 ms, which is consistent with the decay constants of 40–60 ms observed in the sub-second radiation. The simulated de-excitation gamma-ray spectra for our detectors, in which the atmosphere, surrounding materials, and detector energy resolution are taken into account, are also found to be consistent with the observed data (Fig. 2). Notably the sharp cutoff at ~ 10 MeV is explained to be caused by the lack of nuclear lines above this energy (see Methods “Neutron capture”).

The other major products ^{13}N and ^{15}O gradually decay into stable ^{13}C and ^{15}N via beta-plus decays, $^{13}\text{N} \rightarrow ^{13}\text{C} + e^+ + \nu_e$ (a half life of 598 s) and $^{15}\text{O} \rightarrow ^{15}\text{N} + e^+ + \nu_e$ (122 s), respectively. A region, or “cloud”, filled with these isotopes emits positrons for more than 10 minutes and moves by wind above our detectors without experiencing much diffusion due to a low mobility of the isotopes. A positron emitted

from ^{13}N or ^{15}O travels in the atmosphere for roughly a few metres, quickly annihilates in meeting an ambient electron, and radiates two 0.511 MeV photons, whose atmospheric mean free path is ~ 89 m. The epoch t_{peak} detected at the detector A is consistent with the wind velocity and direction at the day (see Fig. 1 and Methods “Ambient wind flow”). The decaying phase ($t < 10$ s, Fig. 3) observed with the detectors A and D is interpreted as a consequence of beta-plus decay of unstable radioisotopes, which were produced around the detectors by the photonuclear reactions at the initial radiation flash (e.g., ^{27}Si in the ground with a half life of 4.15 s).

Here we estimate the densities of positrons and neutrons generated by the lightning with a help of Monte Carlo simulations, on the basis of the photonuclear reactions and subsequent physical processes. We find with our simulations that the obtained annihilation spectrum is well explained by the cloud located ~ 80 m away from the detector (see Methods “Positrons and annihilation”). Since the number of the delayed 0.511 MeV photons obtained by the detector A is $N_{511} = (1.4 \pm 0.2) \times 10^3$ during the period $\Delta t = 52$ s for $11 < t < 63$ s, the corresponding time-integrated beta-plus-decay density for the period is estimated to be $n_{\beta+} = 3.1 \times 10^{-3} \text{ cm}^{-3}$, assuming a simplified cylindrical volume V for the cloud with a horizontal radius $R_d = 220$ m (see Methods “Ambient wind flow”) and fiducial vertical discharge length $L_d = 1 \text{ km}$ ^{23,28,29}. Using the number densities $n_{^{13}\text{N}}$ and $n_{^{15}\text{O}}$ with decay constants $\lambda_{^{13}\text{N}}$ and $\lambda_{^{15}\text{O}}$ of ^{13}N and ^{15}O , respectively, the beta-plus decay rate is given by $S_{\beta+}(t) = \lambda_{^{13}\text{N}}n_{^{13}\text{N}}(t) + \lambda_{^{15}\text{O}}n_{^{15}\text{O}}(t)$. In our estimation (see Methods “Contribution from oxygen”), positrons emitted by ^{15}O amounts 44% of those by ^{13}N at $t_{\text{peak}} = 35$ s. Combining them with the relation $S_{\beta+}\Delta t = n_{\beta+}$, we derive $n_{^{13}\text{N}} = 1.6 \times 10^{-2} \text{ cm}^{-3}$ at t_{peak} , and the initial number density of isotopes of $n_0 = n_{^{13}\text{N}}(0) + n_{^{15}\text{O}}(0) = 2.6 \times 10^{-2} \text{ cm}^{-3}$. Consequently, the total number of the produced neutrons is

$$N_n = n_0V = 4 \times 10^{12} \left(\frac{R_d}{220 \text{ m}} \right)^2 \left(\frac{L_d}{1.0 \text{ km}} \right), \quad (1)$$

which is within the theoretically predicted range of $N_n = 10^{11-15}$ from the TGF studies^{17,19}.

Since the discovery of TGFs with an energy of as high as 20–30 MeV or more, the potential nuclear reactions in lightning have been hotly discussed^{12,16–19}, but have never been observationally confirmed before. We have presented the first unequivocal observational evidence for nuclear reactions triggered by lightning. In fact, we have once detected a similar event before; however, the result was marginal at best due to limited observational information available at that time²⁶ (see Methods “Comparison with the similar event”). This finding pioneers a research field of atmospheric nuclear reactions in lightning studied by positrons and neutrons from the ground. More importantly, these reactions in lightning provide a previously-unknown natural channel on the Earth to generate isotopes of carbon, nitrogen, and oxygen (^{13}C , ^{14}C , ^{13}N , ^{15}N , and ^{15}O). The short-lived isotopes ^{13}N and ^{15}O emit positrons over our heads, of which humans have never been aware before, whereas more stable ^{13}C , ^{14}C , and ^{15}N contribute to the natural isotope composition on the Earth, albeit for a small fraction. Humans knew up to now only two natural origins of carbon isotopes on the Earth; stable primordial isotopes ^{13}C from geological time, originating from the stellar nucleosynthesis³⁰, and semi-stable ^{14}C produced via atmospheric interactions

with cosmic rays. Our discovery adds nuclear reactions in lightning as another origin for them.

Methods

GROWTH collaboration. The Gamma-Ray Observation of Winter Thunderclouds (GROWTH) project is a collaboration to study the high-energy radiation from lightning and thunderstorms, starting in 2006^{7,25}. The site of our experiment, Kashiwazaki-Kariwa nuclear power station, is located at (37.4267° N, 138.6014° E) in latitude and longitude and at an altitude of ~ 30 –40 m. We have detected 14 unequivocal events of minute-long gamma-ray enhancements from thunderclouds as of 2017 August^{7,25}. The detectors operated during the winter in 2016–2017 are summarised in Table 1. Among them, the detectors A–C were newly deployed in 2016; they use a $25 \times 8 \times 2.5$ cm³ BGO (Bi₄Ge₃O₁₂) scintillation crystal, with two photomultiplier tubes (PMTs) HAMAMATSU R1924A attached to for each. Signals are read out via analogue circuits connected to a new ADC board developed with a crowdfunding support. The detector D has been operated since 2010, and consists of a 7.62 cm \times ϕ 7.62 cm NaI scintillation crystal with a PMT R6231 attached to. Signals of the detector D are read out via another analogue circuit. In each detector, individual radiation events are recorded with time and pulse height. The effective areas are determined to be 149 and 28 cm² at 0.511 MeV for the detectors A–B and D, respectively, with the Monte Carlo simulation using Geant4³¹, in which irradiated photons are monochromatic at 0.511 MeV. The environmental electric-field was monitored at the position of the detector D.

Lightning discharges. On 6 February 2017, the Japan lightning-detection network, operated by Franklin Japan Co. Ltd, recorded a negative discharge, in which the positive ground charge and negative one in the cloud cancelled each other, at 08:34:06.002716165 UTC at (37.432° N, 138.590° E) with a peak current of -33 kA. The subsequent positive discharge occurred 23.7 μ s later at (37.428° N, 138.588° E) with a +44 kA peak current.

An associated electromagnetic signal was confirmed in the frequency range of 1–100 Hz (ELF range) at the Kuju station (33.059° N, 131.233° E) in Japan, which is located ~ 830 km southwest from the position of the lightning (Fig. 5). This ELF observation supports that the two bipolar cloud-to-ground discharges occurred simultaneously with this event.

Initial flash. All our detectors A–D detected a very strong bursting event almost coincidentally with the lightning (Fig. 1). The detectors A–C digitise the waveform of an analogue pulse of the PMT output for 20 μ s once the pulse height exceeds the trigger threshold, and record the highest and the lowest values. The former is used to measure the energy of the pulse signal, while the latter can be used to monitor the analogue baseline voltage. In contrast, the detector D has a different analogue circuit from the others and does not provide direct information of the baseline voltage, which is crucial in this case as discussed below. For that reason, we exclude the data with the detector D for the initial 1 second of the event in our analysis.

At the initial stage of the recorded event, we noticed that their baseline voltages were significantly negative. The level of the baseline gradually settled down to the nominal value in 20–40 ms (Fig. 6). This is abnormal, and can not be some technical glitch in the system, given that the detectors are completely separate, located hundreds of metres apart from one another.

The most plausible interpretation is that the detectors received an extremely strong signal with the intensity beyond the maximum that they are able to measure, lasting for much shorter than 1 ms, and then caused the peculiar analogue undershoot lasting for ~ 10 ms. At laboratory we made follow-up experiments using the detectors A–C to simulate what these detectors should have experienced at the lightning; we applied a bias voltage of 1100 V which is higher than the one set during the field observation (~ 900 V) to raise the PMT gain by a factor of ~ 5 . In this configuration, a cosmic-ray muon-penetration signals equivalent to 30–50 MeV energy deposit is amplified to 150–250 MeV gamma-ray-equivalent charge-output. We observed the “peculiar” undershoot with an intensity up to -1000 ADC channel and a recovery time constant (~ 1 ms), both of which are very similar to what were observed in the lightning event by the detectors B and C. This result confirms the interpretation; there must have been, though not directly measured with our detectors, an initial strong radiation flash at the lightning. In fact, the detector A detected ~ 10 events with energies above 10 MeV at the very beginning (< 2 ms) of the flash, before the onset of the undershoot. The detection further reinforces this interpretation.

In the detector A, the undershoot lasted longer than in the other two. The level of the undershoot at $t = 40$ ms is equivalent to an energy shift of ~ -0.5 MeV, which changes the energy scale by $> 50\%$ below 1 MeV, but only by $\sim 5\%$ at 10 MeV. To minimise the effect of this energy-scale shift, we extracted and plotted spectra of the sub-second decaying radiation above 1 MeV in Fig. 2.

Radiation monitors. Radiation monitors are installed in the site at ~ 300 – 400 m intervals (Fig. 1) and are operated at all times. Each radiation monitor has a spherical ion chamber (IC) filled with ~ 14 L argon gas, and covers an energy range above 3 MeV with a coarse time resolution of 30 s.

Instrumental calibration. Energy calibrations are performed by a linear fitting of the persistent environmental background emission-lines (e.g., Fig. 2) of ^{40}K (1.461 MeV) and ^{208}Tl (2.615 MeV). We perform this calibration procedure for the detectors A–C every 30 min in order to correct the sensitive temperature dependency of light yields of the BGO scintillation crystals ($\sim 1\%$ per degree Celsius), whereas we do it daily for the NaI of the detector D. We evaluate the uncertainty of this energy calibration, using another background emission line of ^{214}Bi at 0.609 MeV, which appears with rainfall as a component of radon wash-out radiation. The measured centre energy fluctuates around 0.609 MeV with a standard deviation of 0.007 MeV. Thus, the energies of individual photons are calibrated down to an accuracy of 1.1% (systematic uncertainty), or ~ 0.006 MeV for 0.511 MeV, in all the detectors A–D.

The information of the absolute timing of individual photons is usually assigned from the data of the Global Positioning System (GPS) signals with a time resolution of $2 \mu\text{s}$, which is the typical time scale of signal waveforms in the detectors A–C. However, the GPS signals were lost during the event

on 6 February. Hence, the time tags were assigned, referring to the internal clock time (Unix time) of our detectors, instead. We verified the absolute timing uncertainties within 1 s for the three detectors A–C, comparing the rising epochs of the initial flash measured with these detectors. The detector D has a 100 μs time resolution, and the absolute time is calibrated within 100 μs , using the successfully received GPS signals during the event.

Neutron propagation. The physical processes that follow the photonuclear reactions are schematically illustrated in Fig. 7. The photonuclear reactions, $^{14}\text{N}(\gamma, n)^{13}\text{N}$ and $^{16}\text{O}(\gamma, n)^{15}\text{O}$, kick out fast neutrons of atmospheric nitrogen and oxygen with a typical kinetic energy of ~ 10 MeV^{12,17–19}. In the following discussion, we only consider the most abundant target ^{14}N , given that the cross section of the second most abundant target ^{16}O is relatively small. The neutron cross section with ^{14}N , shown in Fig. 8a, has three main processes: elastic scattering, charged-particle production $^{14}\text{N}(n, p)^{14}\text{C}$, and radiative neutron capture $^{14}\text{N}(n, \gamma)^{15}\text{N}$. Incident fast neutrons gradually lose their kinetic energy via multiple elastic scatterings, whose microscopic cross-section is almost independent of energy $\sigma_{\text{es}} \sim 10$ barns^{32,33} for 0.01–10⁴ eV, and is much larger than that of the other two processes. As neutrons are moderated and diffused to the epithermal energy (~ 0.1 –100 eV), the cross sections of charged-particle production and neutron capture gradually increase, and neutrons disappear.

The neutron moderation is in a similar situation to some nuclear engineering³⁴. Let *lethargy* ξ be the logarithm of the inverse ratio of the change of neutron kinetic energy in a single elastic scattering, from E_n to E_{n+1} , where E_n is the energy after n scatterings. It is approximated as $\xi = \ln(E_n/E_{n+1}) \sim 2/(A + 2/3) = 0.136$, where $A = 14$ is the nitrogen mass number. Since the energy deposit in a single scattering is $\Delta E = E_n - E_{n+1} = (1 - e^{-\xi})E_n = 0.127E_n$, the neutron energy decreases from the initial energy E_0 as $E_n = 0.873^n E_0$. At each scattering, a mean free path λ is almost independent of the neutron energy³⁴,

$$\lambda = 23.8 \text{ m} \left(\frac{\sigma_{\text{es}}}{10 \text{ barns}} \right)^{-1} \left(\frac{\rho}{10^{-3} \text{ g cm}^{-3}} \right)^{-1} \left(\frac{A}{14} \right)^{-1}, \quad (2)$$

where ρ is the atmospheric nitrogen density. Therefore, the duration between the two contiguous scatterings is $\Delta t_n = \lambda \sqrt{m_n/2E_n}$, where m_n is the neutron rest mass energy ($m_n = 940$ MeV). The elapsed time until the n -th scattering is $t_n = \sum_{n'} \Delta t_{n'}$. The number of the neutrons N_n after the n -th scattering decreases with a loss in the mean free path λ of $\Delta N_n = N_n \{1 - \exp[-(\sigma_{\text{np}} + \sigma_{\text{cap}})/\sigma_{\text{es}}]\}$, where σ_{np} and σ_{cap} are the cross sections of charged-particle production and neutron capture, respectively. Numerically solving for E_n , t_n , and ΔN_n with n (Fig. 8b), the number of the surviving neutrons at t for 5–200 ms is approximately $N(t) = N(0) \exp(-t/\tau_n)$ with the decay constant of $\tau_n = 56$ ms. Therefore, the neutron disappearing rate via capture is

$$\frac{dN_{\text{cap}}}{dt} = \frac{\sigma_{\text{cap}}}{\sigma_{\text{np}} + \sigma_{\text{cap}}} \frac{d}{dt} N(t) \propto \exp\left(-\frac{t}{\tau_n}\right). \quad (3)$$

The theoretically-calculated ($\tau_n \sim 56$ ms) and observed (40–60 ms) decay constants are found to be consistent with each other. In addition, assuming isotropic random-walk scatterings, the diffusion distance

σ_d is estimated to be

$$\sigma_d \sim \lambda \sqrt{n} = 260 \text{ m} \left(\frac{\lambda}{23.8 \text{ m}} \right) \left(\frac{n}{120} \right)^{1/2}. \quad (4)$$

It is in the same order as the distance between our detectors and the lightning discharges.

Neutron capture. Moderated neutrons are captured by nuclei in the atmosphere, surrounding materials, or detectors. Then the nucleus promptly radiates several gamma-ray photons at discrete energies below ~ 10 MeV within nanoseconds. We simulated the expected gamma-ray spectra with Geant4 Monte Carlo simulations. We implemented the BGO scintillation crystals, aluminium plates of supporting jigs, a detector box made of Acrylonitrile Butadiene Styrene (ABS) resin and polycarbonate, and lead blocks below them. The detectors were placed on a 1-m thick flat concrete ground, which imitates the building, and in the atmosphere with a uniform density of $1.2 \times 10^{-3} \text{ g cm}^{-3}$, composed of nitrogen (75.527% in weight fraction), oxygen (23.145%), argon (1.283%), and carbon dioxide (0.045%). De-excitation gamma rays with an energy above 0.1 MeV and branching ratio $> 10\%$ for the strongest line were generated isotropically and uniformly from atmospheric nitrogen (^{14}N), surrounding materials (^{27}Al , ^{28}Si , and ^{207}Pb), and the BGO crystal itself (^{70}Ge , ^{72}Ge , ^{74}Ge , and ^{209}Bi), according to the branching ratios from Evaluated Nuclear Structure Data File (ENSDF) database (<http://www.nndc.bnl.gov/ensdf/>). We compared the observed spectra of the detectors A–C with the simulated ones (Fig. 9), and found that the cylindrical source geometry with a horizontal radius of $R_d = 220$ m and a vertical length of $L_d = 1$ km can reproduce the spectrum with the detector A. In contrast, a source ~ 300 m away from the detectors consisting solely of the nitrogen contribution was found to roughly reproduce the spectra with the detectors B and C. These results indicate that neutrons hit matters surrounding the detector A, while only de-excitation gamma rays from the atmospheric nitrogen reached the detectors B and C.

Ambient wind flow. The ambient wind flow at an altitude of 85 m was northwesterly (Fig. 1) with a velocity of $v_w = 17 \text{ m s}^{-1}$, and was constant within $\pm 1 \text{ m s}^{-1}$ during the event, according to a weather monitor near the detector D, operated by the nuclear power station. The wind information was also confirmed with the weather radar images from Japan Meteorological Agency (Fig. 5b–d). The time profile of the delayed annihilation signal (Fig. 3c) is approximated by a Gaussian with a peak time of $t_{\text{peak}} = 34.5 \pm 1.0$ s and a duration of $\sigma_t = 13.2 \pm 1.0$ s (1σ). The drifting distance of the positron-emitting cloud during the period of $0-t_{\text{peak}}$ is then calculated to be $v_w t_{\text{peak}} \sim 590$ m. It is comparable with the separation between the detector A and the place of the discharges. The wind direction is also consistent with our interpretation. A typical horizontal size (radius) of the cloud is estimated from the duration to be

$$R_d = v_w \sigma_t \sim 220 \text{ m} \left(\frac{v_w}{17 \text{ m s}^{-1}} \right) \left(\frac{\sigma_t}{13.2 \text{ s}} \right). \quad (5)$$

Positrons and annihilation. We here examine positron emission from radioactive isotopes and 0.511 MeV annihilation line-emission. Positrons are isotropically emitted with continuous energy spectra following the beta-plus formula with maximum kinetic energies of 1.19 MeV and 1.72 MeV from ^{13}N and ^{15}O , respectively. Roughly 97% of positrons with an initial kinetic energy of ~ 1 MeV annihilate with non-

relativistic electrons via positronium formation, after losing their kinetic energy within a few metres by ionising ambient atoms, and subsequently emit two back-to-back 0.511 MeV photons. The remaining $\sim 3\%$ directly annihilate in flight (direct annihilation of relativistic positrons³⁵) and emit two photons with energies between $\sim m_e c^2/2$ and $\sim E + 3m_e c^2/2$, where $m_e c^2$ and E are the rest mass and kinetic energies of positron, respectively. These photons from direct annihilation by nitrogen- and oxygen-origin positrons make a weak continuum up to ~ 2.0 MeV and ~ 2.5 MeV, respectively.

In order to examine the expected spectrum from annihilation processes, we performed Geant4 Monte Carlo simulations using the similar setup of de-excitation gamma-ray simulations. We assumed a cylindrical positron-emitting cloud with various distances to its base. Positrons were generated isotropically and uniformly inside the source volume, with a continuum energy distribution of the beta-plus decay, taking into account the proportion of the contributions from ^{13}N and ^{15}O . Fig. 10 shows the resultant simulated spectra. We then compared this simulation with the observed delayed annihilation signal (Fig. 4), and found that the model with the cloud-base distance of 80 m reproduce the observed data best. Using this distance, we calculated the conversion factor of the number of beta-plus decays in a unit volume to the detected annihilation photons at the 0.511 MeV line to be $N_{511}/n_{\beta+} = 4.5 \times 10^5 \text{ cm}^3$, assuming the horizontal radius $R_d = 220$ m (see Methods “Ambient wind flow”). The total number of beta-plus decay events in a unit volume is calculated to be $n_{\beta+} = 3.1 \times 10^{-3} \text{ cm}^{-3}$ from the observed number of delayed annihilation signals $N_{511} = 1.4 \times 10^3$.

Contribution from oxygen. The two dominant targets of the photonuclear reactions in the atmosphere are ^{14}N and ^{16}O . Here we assume the incident gamma-ray spectrum to have the same shape as that in the past reported TGFs, which is $N(E) \propto E^{-\Gamma} \exp(-E/E_c)$ for the photon energy E , photon index $\Gamma = 1.4$, and cutoff energy $E_c = 6.6$ MeV¹⁵. Then, the event-number ratio η_{prod} of the photonuclear reactions with ^{16}O to that with ^{14}N is estimated to be $\eta_{\text{prod}} = 10.4\%$, when integrated for the energies of seed gamma rays up to ~ 28 MeV, using the atmospheric abundances of nitrogen (78.08%) and oxygen (20.94%), and the experimental cross sections (e.g., ~ 15 mb and ~ 10 mb for ^{14}N and ^{16}O at ~ 23 MeV, respectively³²). The event rates per unit time of the subsequent beta-plus decays also differ, due to a difference of the decay constants between the two isotopes; the half-lives of 597.9 and 122.2 sec for ^{13}N and ^{15}O correspond with the decay constants of $\lambda_{^{13}\text{N}} = 1.16 \times 10^{-3} \text{ s}^{-1}$ and $\lambda_{^{15}\text{O}} = 5.67 \times 10^{-3} \text{ s}^{-1}$, respectively. These give the decay rates to be $dN_{^{13}\text{N}}(t)/dt = \lambda_{^{13}\text{N}} \exp(-\lambda_{^{13}\text{N}}t)$ and $dN_{^{15}\text{O}}(t)/dt = \lambda_{^{15}\text{O}} \exp(-\lambda_{^{15}\text{O}}t)$ for ^{13}N and ^{15}O , respectively. Therefore, the ratio of the contribution of the annihilation signal of the positrons from ^{15}O to that from ^{13}N is

$$\eta(t) = \eta_{\text{prod}} \frac{dN_{^{15}\text{O}}(t)/dt}{dN_{^{13}\text{N}}(t)/dt} = \eta_{\text{prod}} \frac{\lambda_{^{15}\text{O}}}{\lambda_{^{13}\text{N}}} \exp[-(\lambda_{^{15}\text{O}} - \lambda_{^{13}\text{N}})t] = 0.51 \exp\left(-\frac{t}{222 \text{ s}}\right). \quad (6)$$

It yields $\sim 44\%$ at $t_{\text{peak}} = 35$ s.

Comparison with the similar event. An event associated with 0.511 MeV emission, similar to the event reported in this paper, was once detected previously at the same site on 13 January, 2012, after a pair of positive and negative discharges²⁶. At the time of the event, only the detector D was operated. The data

acquisition was heavily hampered by the analogue undershoot for ~ 200 ms, thus studying the sub-second radiation with de-excitation spectra was impossible. In addition, since the electric-field monitor was not working at that time, we were unable to eliminate the pair production scenario entirely. In contrast, in the event reported in this paper, we measured the environmental electric-field at the place of the detector D, using a commercial electric field mill BOLTEK EFM-100, and found it to be negative during the delayed (annihilation) phase, which implies that electrons moved to the ground away from negatively charged clouds, and thus generating the 0.511 MeV line without emitting 10–20 MeV bremsstrahlung photons is impossible.

1. Dwyer, J. R., Smith, D. M. & Cummer, S. A. High-energy atmospheric physics: Terrestrial gamma-ray flashes and related phenomena. *Space Science Reviews* **173**, 133–196 (2012).
2. Gurevich, A. V., Milikh, G. M. & Roussel-Dupre, R. Runaway electron mechanism of air breakdown and preconditioning during a thunderstorm. *Physics Letters A* **165**, 463–468 (1992). URL <http://www.sciencedirect.com/science/article/pii/037596019290348P>.
3. Dwyer, J. R. The relativistic feedback discharge model of terrestrial gamma ray flashes. *Journal of Geophysical Research (Space Physics)* **117**, A02308 (2012).
4. Moore, C. B., Eack, K. B., Aulich, G. D. & Rison, W. Energetic radiation associated with lightning stepped-leaders. *Geophysical Research Letters* **28**, 2141–2144 (2001). URL <http://dx.doi.org/10.1029/2001GL013140>.
5. Torii, T., Takeishi, M. & Hosono, T. Observation of gamma-ray dose increase associated with winter thunderstorm and lightning activity. *Journal of Geophysical Research: Atmospheres* **107**, 4324 (2002).
6. Dwyer, J. R. *et al.* A ground level gamma-ray burst observed in association with rocket-triggered lightning. *Geophysical Research Letters* **31**, L05119 (2004).
7. Tsuchiya, H. *et al.* Detection of high-energy gamma rays from winter thunderclouds. *Physical Review Letters* **99**, 165002 (2007). 0708.2947.
8. Chilingarian, A. *et al.* Ground-based observations of thunderstorm-correlated fluxes of high-energy electrons, gamma rays, and neutrons. *Phys. Rev. D* **82**, 043009 (2010). URL <https://link.aps.org/doi/10.1103/PhysRevD.82.043009>.
9. Dwyer, J. R. *et al.* Observation of a gamma-ray flash at ground level in association with a cloud-to-ground lightning return stroke. *Journal of Geophysical Research: Space Physics* **117**, A10303 (2012).
10. McCarthy, M. & Parks, G. K. Further observations of x-rays inside thunderstorms. *Geophysical Research Letters* **12**, 393–396 (1985). URL <http://dx.doi.org/10.1029/GL012i006p00393>.

11. Eack, K. B., Beasley, W. H., Rust, W. D., Marshall, T. C. & Stolzenburg, M. Initial results from simultaneous observation of x-rays and electric fields in a thunderstorm. *Journal of Geophysical Research: Atmospheres* **101**, 29637–29640 (1996). URL <http://dx.doi.org/10.1029/96JD01705>.
12. Dwyer, J. R. *et al.* Positron clouds within thunderstorms. *Journal of Plasma Physics* **81**, 475810405 (2015). 1505.03782.
13. Fishman, G. J. *et al.* Discovery of intense gamma-ray flashes of atmospheric origin. *Science* **264**, 1313–1316 (1994).
14. Smith, D. M., Lopez, L. I., Lin, R. P. & Barrington-Leigh, C. P. Terrestrial gamma-ray flashes observed up to 20 Mev. *Science* **307**, 1085–1088 (2005).
15. Tavani, M. *et al.* Terrestrial gamma-ray flashes as powerful particle accelerators. *Phys. Rev. Lett.* **106**, 018501 (2011). URL <https://link.aps.org/doi/10.1103/PhysRevLett.106.018501>.
16. Babich, L. P. Neutron generation mechanism correlated with lightning discharges. *Geomagnetism and Aeronomy* **47**, 664–670 (2007).
17. Carlson, B. E., Lehtinen, N. G. & Inan, U. S. Neutron production in terrestrial gamma ray flashes. *Journal of Geophysical Research: Space Physics* **115**, A00E19 (2010).
18. Babich, L. P., Bochkov, E. I., Kutsyk, I. M. & Rassoul, H. K. Analysis of fundamental interactions capable of producing neutrons in thunderstorms. *Phys. Rev. D* **89**, 093010 (2014).
19. Babich, L. P., Bochkov, E. I., Kutsyk, I. M. & Roussel-Dupré, R. A. Localization of the source of terrestrial neutron bursts detected in thunderstorm atmosphere. *Journal of Geophysical Research: Space Physics* **115** (2010). URL <http://dx.doi.org/10.1029/2009JA014750>. A00E28.
20. Fleischer, R. L. Search for neutron generation by lightning. *Journal of Geophysical Research* **80**, 5005–5009 (1975). URL <http://dx.doi.org/10.1029/JC080i036p05005>.
21. Shah, G. N., Razdan, H., Ali, Q. M. & Bhat, C. L. Neutron generation in lightning bolts. *Nature* **313**, 773–775 (1985).
22. Shyam, A. & Kaushik, T. C. Observation of neutron bursts associated with atmospheric lightning discharge. *Journal of Geophysical Research: Space Physics* **104**, 6867–6869 (1999). URL <http://dx.doi.org/10.1029/98JA02683>.
23. Rakov, V. & Uman, M. *Lightning: Physics and Effects* (Cambridge University Press, 2003). URL <https://books.google.co.jp/books?id=TuMa5lAa3RAC>.

24. Goto, Y. & Narita, K. Observations of winter lightning to an isolate tower. *Res. Lett. Atmos. Electr.* **12**, 57–60 (1992).
25. Tsuchiya, H. *et al.* Long-duration γ ray emissions from 2007 and 2008 winter thunderstorms. *Journal of Geophysical Research: Atmospheres* **116**, D09113 (2011). 1102.4024.
26. Umemoto, D. *et al.* On-ground detection of an electron-positron annihilation line from thunderclouds. *Physical Review E* **93** (2016).
27. Hare, B. M. *et al.* Ground-level observation of a terrestrial gamma ray flash initiated by a triggered lightning. *Journal of Geophysical Research: Atmospheres* **121**, 6511–6533 (2016). URL <http://dx.doi.org/10.1002/2015JD024426>. 2015JD024426.
28. Chen, L., Zhang, Q., Hou, W. & Tao, Y. On the field-to-current conversion factors for large bipolar lightning discharge events in winter thunderstorms in Japan. *Journal of Geophysical Research: Atmospheres* **120**, 6898–6907 (2015). URL <http://dx.doi.org/10.1002/2015JD023344>. 2015JD023344.
29. Wu, T. *et al.* Large bipolar lightning discharge events in winter thunderstorms in Japan. *Journal of Geophysical Research: Atmospheres* **119**, 555–566 (2014). URL <http://dx.doi.org/10.1002/2013JD020369>. 2013JD020369.
30. Woosley, S. E. & Weaver, T. A. The evolution and explosion of massive stars. ii. explosive hydrodynamics and nucleosynthesis. *Astrophysical Journal Supplement* **101**, 181 (1995).
31. Agostinelli, S. *et al.* Geant4 - a simulation toolkit. *Nuclear Instruments and Methods in Physics Research, Section A: Accelerators, Spectrometers, Detectors and Associated Equipment* **506**, 250–303 (2003). 1005.0727v1.
32. Agency, I. A. E. *Handbook on Photonuclear Data for Applications: Cross-sections and Spectra: Final Report of a Co-ordinated Research Project 1996-1999*. IAEA-Tecdoc (IAEA, 2000). URL <https://books.google.co.jp/books?id=BvLejgEACAAJ>.
33. Shibata, K. *et al.* JENDL-4.0: A new library for nuclear science and engineering. *Journal of Nuclear Science and Technology* **48**, 1–30 (2011). URL <http://www.tandfonline.com/doi/abs/10.1080/18811248.2011.9711675>.
34. Lamarsh, J. R. & Baratta, A. J. *Introduction to Nuclear Engineering 3rd Edition*. 3rd, Third, 3e Year: 2001 Format: Hardcover 783 pages (IAEA, 2001). URL <https://www.pearson.com/us/higher-education/program/Lamarsh-Introduction-to-Nuclear-Engineering-3rd-Edition/PGM92364.html>.

35. Prantzos, N. *et al.* The 511 keV emission from positron annihilation in the galaxy. *Reviews of Modern Physics* **83**, 1001–1056 (2011). 1009.4620.

Acknowledgements We thank the members of the radiation safety group of the Kashiwazaki-Kariwa nuclear power station, TEPCO Inc. for providing observation sites, Dr. Hiroko Miyahara, Dr. Norita Kawanaka, and Dr. Hideaki Ohgaki for helpful discussions, Dr. Hiroyoshi Sakurai, Dr. Megumi Niikura, and the Sakurai group members at RIKEN Nishina Center for providing BGO scintillation crystals, Dr. Toru Tamagawa for his project support, Mr. Gregory Bowers, Dr. Masashi Kamogawa, and Dr. David Smith for their helpful suggestion to our interpretation, Mr. Shigemi Otsuka and Mr. Hiroshi Kato for supporting the detector developments, and RIKEN Advanced Center for Computing and Communication for use of HOKUSAI GreatWave supercomputing system for Monte Carlo simulations. This research is supported by JSPS/MEXT KAKENHI grant numbers 15K05115, 15H03653, and 16H06006, by SPIRITS 2019 of Kyoto University, and by the joint research program of the Institute for Cosmic Ray Research (ICRR), the University of Tokyo. Our project is also supported by crowdfunding named Thundercloud Project, using the academic crowdfunding platform “academist”, and we express our sincere gratitude to Yutaka Shikano, Yasuyuki Araki, Makoto T. Hayashi, Nobuo Matsumoto, Takeaki Enoto, Katsuhiko Hayashi, Sumitaka Koga, Takashi Hamaji, Yu-suke Torisawa, Sadashi Sawamura, Jim Purser, Shozo Suehiro, Sumio Nakane, Masahiro Konishi, Hajime Takami, and Tomoo Sawara, and all the backers of Thundercloud Project. The data of Himawari 8 in Fig. 5a was obtained from Science cloud of National Institute of Information and Communications Technology (NICT), Data Integration and Analysis System Program (DIAS) by the University of Tokyo, Center for Environmental Remote Sensing (CEReS) of Chiba University, and Earth Observation Research Center of Japan Aerospace Exploration Agency. The data of Fig. 5b–d was supplied from Japan Meteorological Agency and downloaded from the website of Research Institute for Sustainable Humanosphere, Kyoto University (<http://database.rish.kyoto-u.ac.jp/index-e.html>).

Author Contributions T.E., Y.W., Y.F., K.O., K.N., T.Y., T.N., and T.H. are responsible for the detector developments, data analyses, and interpretation; T.E. is the project leader and wrote the draft of the manuscript; Y.W. made a major contribution to the detector development, installation, and in particular, analysis; Y.F. led the Monte Carlo simulations using Geant4; K.N. led the installation of the instruments at Kashiwazaki-Kariwa in 2016; T.Y. led the development of new data acquisition system after 2015; D.U. provided the previous data in 2012; M.S., Y.S., K.M., and H.T. contributed to the data interpretation.

Author Information The authors declare no competing financial interests. Correspondence and requests for materials should be addressed to T.E. (email: teruaki.enoto@gmail.com).

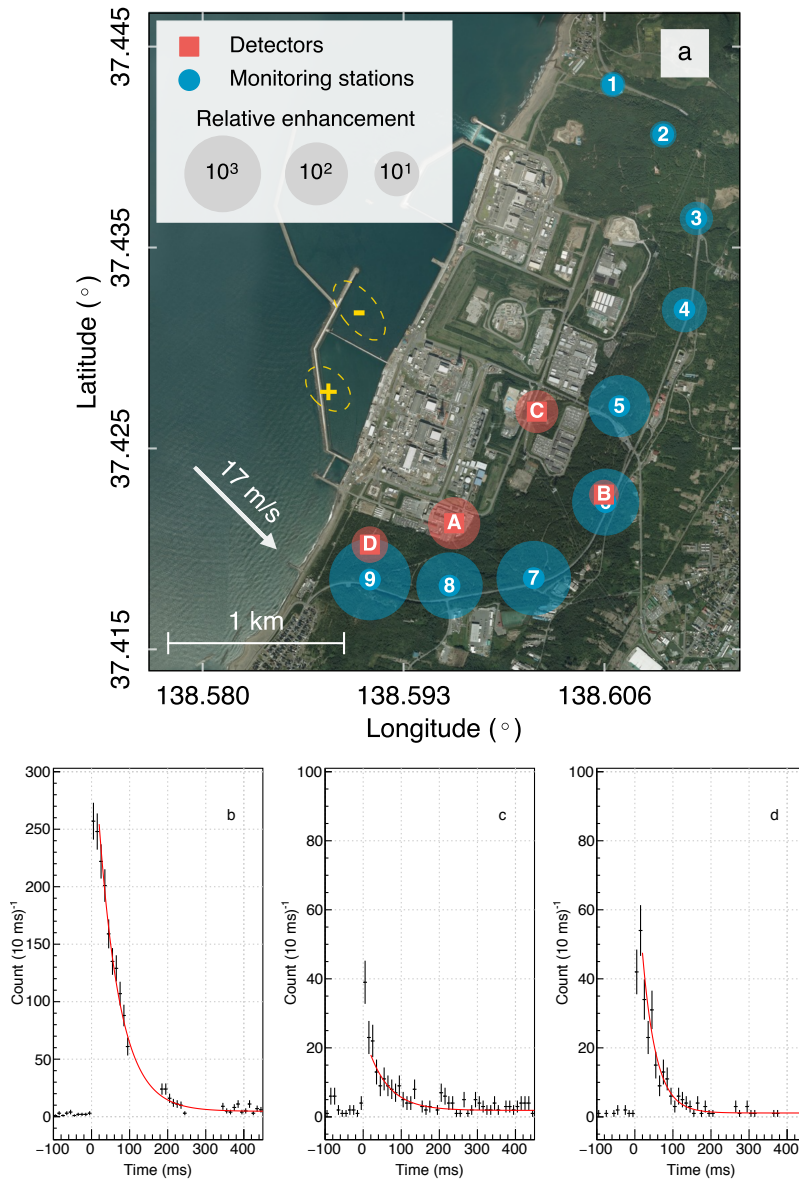


Figure 1: Lightning discharges and associated sub-second decaying high-energy radiation. **a**, Aerial photograph of our observation site, Kashiwazaki-Kariwa, Niigata. The two yellow dashed-lines show the positional error circles of the negative (“-” symbol) and positive (“+”) cloud-to-ground discharges. The red square and blue circles show the locations of our radiation detectors and radiation-monitoring stations, respectively. The radius and the values in the legend of the overlaid circle on each point represents the intensity of the radiation enhancement at the lightning, relative to the environmental backgrounds averaged over ~ 10 min before and after the event. The arrow shows the local wind direction at the time of the lightning. **b–d**, 10-ms-binned count-rate histories (black crosses for $\pm 1\sigma$ errors) before and after the lightning (the time origin of the panels), with the detectors A (panel **b**, > 0.35 MeV), B (**c**, > 0.35 MeV), and C (**d**, > 1.2 MeV). Red lines show the best-fitting model functions of an exponential decay. The data loss due to dead time is corrected in the detector A, whereas the baseline undershoot is corrected for none of the detectors (see Methods “Initial flash”). The data gap for the detector A is due to overflow of memory buffer in the ADC board. The detector D is not used here due to the undershoot (see Methods “Initial flash”).

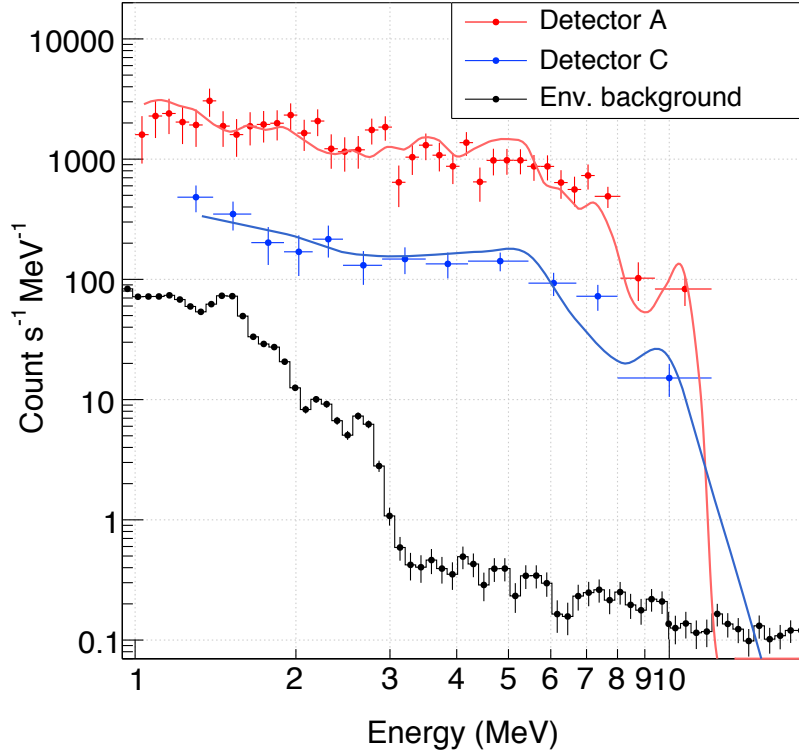


Figure 2: **De-excitation gamma-ray spectra of the sub-second decaying radiation.** Background-subtracted radiation spectra of the detectors (red crosses) A and (blue) C, compared with the simulated de-excitation gamma-ray spectra (solid lines). The events are accumulated over $40 < t < 100$ ms and $20 < t < 200$ ms, respectively. The background spectrum is also plotted for comparison, extracted from $-10 < t < -130$ s and $90 < t < 210$ s. The read-out dead time is corrected for the detector A, whereas the instrumental response is inclusive. The error bars are in $\pm 1\sigma$.

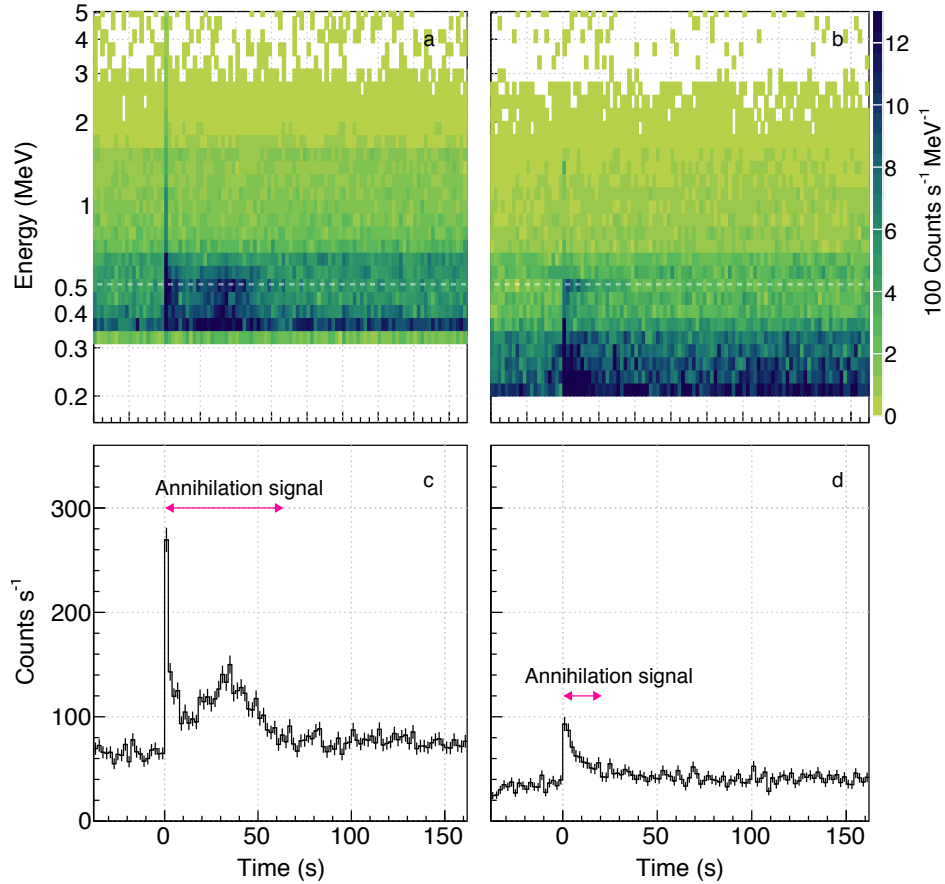


Figure 3: **Count-rate histories during the annihilation signal.** **a, b,** The gradient coloured maps show the detected counts in a unit time and energy (counts s⁻¹ MeV⁻¹) on the two-dimensional histograms of time (abscissa, 1-s binning) and energy (ordinate) for the detectors A (panel **a**) and D (**b**). The horizontal white dashed-line indicates 0.511 MeV. The dominant backgrounds above and below 3 MeV are cosmic-ray induced components and radiation from environmental radioactive nuclei, respectively. **c, d,** 2-s-binned count-rate histories of the 0.35–0.60 MeV band of the detectors A (panel **c**) and D (**d**). Pink arrows in the panels **c** and **d** indicate the time durations of $1.0 < t < 63$ s and $1.0 < t < 20$ s, respectively, from which the annihilation signals were detected and the spectra (Fig. 4) are accumulated. The error bars are in $\pm 1\sigma$.

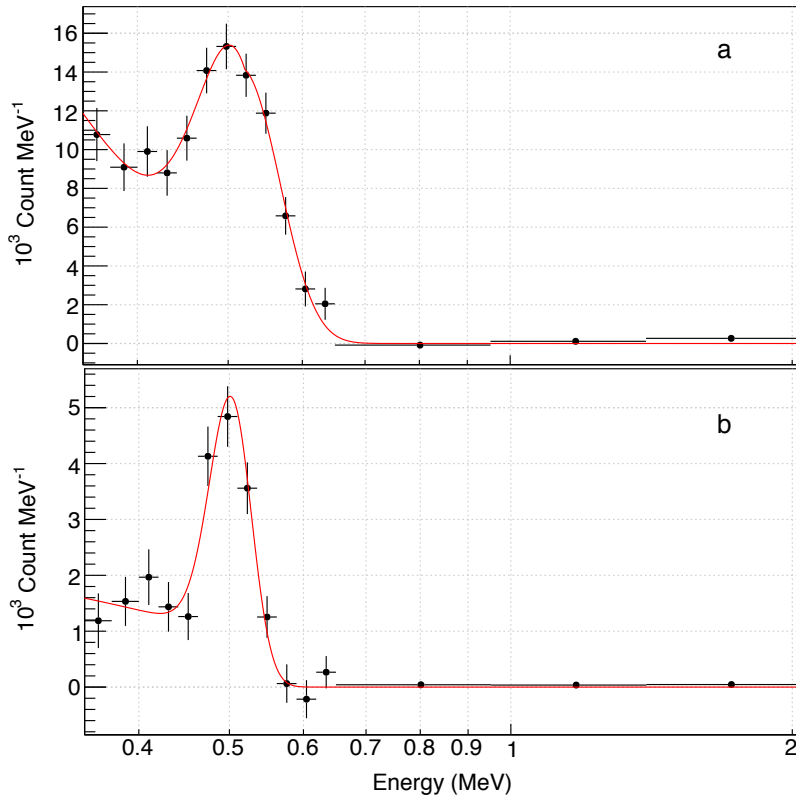


Figure 4: **Gamma-ray spectra during the prolonged annihilation signal.** Panels **a** and **b** are for the detectors A and D, respectively. The background is subtracted from the same time span of Fig. 2. The detector response is inclusive. The error bars are in $\pm 1\sigma$. See the panels **c** and **d** in Fig. 3 for the event-accumulating time regions for the detectors A and D, respectively. Red lines show the best-fitting empirical models consisting of a Gaussian line profile plus a power-law continuum, the latter of which represents the Compton scattering component from the former (see also Methods “Positrons and annihilation” for a physically-based model).

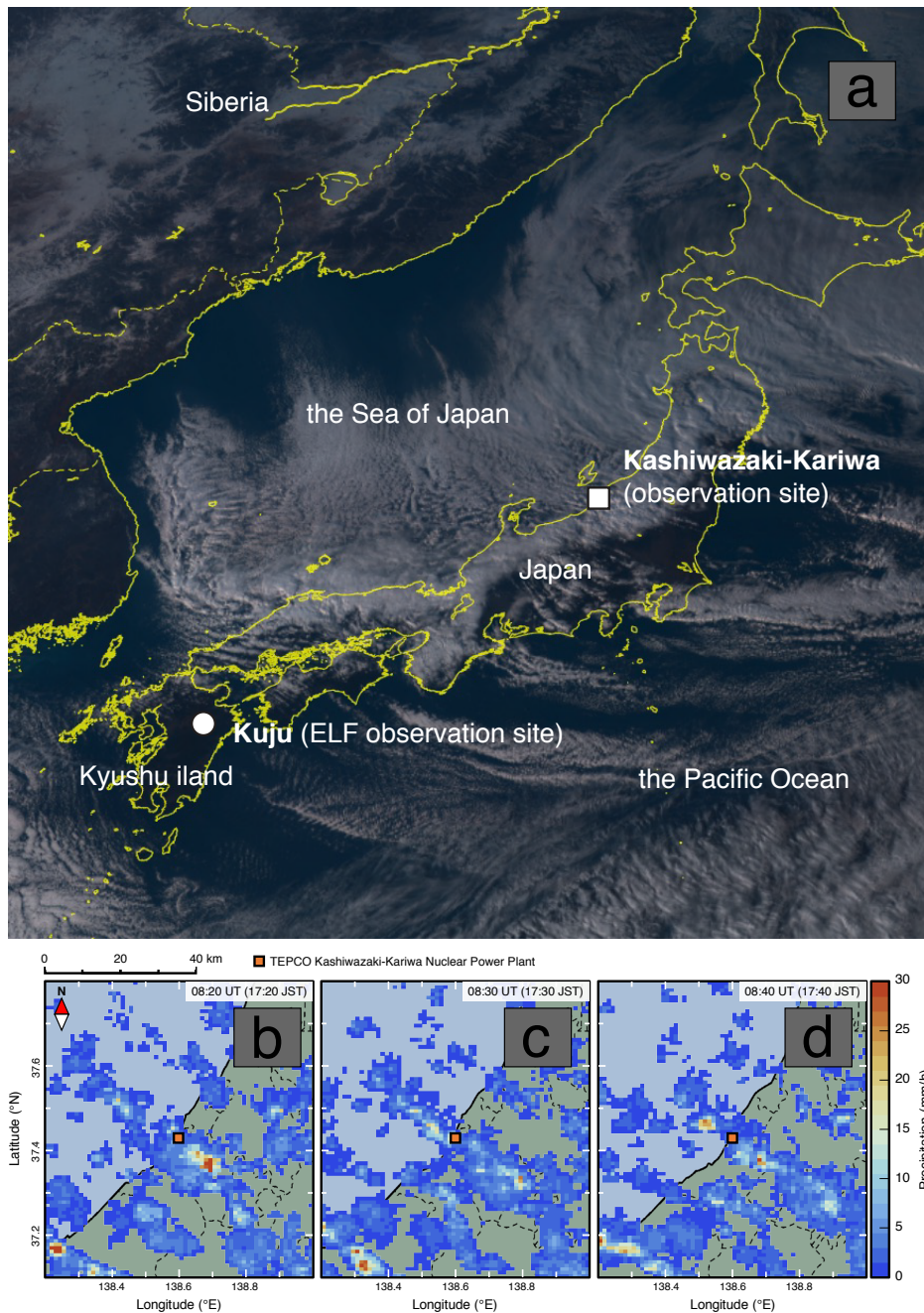


Figure 5: **Location of the observation sites.** **a**, Visible image of the geostationary satellite Himawari 8 at 06:00 UTC on 6 February 2017. The square and circle symbols indicate Kashiwazaki-Kariwa and Kuju, respectively. **b–d**, Precipitation intensity map between 08:20–08:40 UTC on the same day, retrieved from the radar system of Japan Meteorological Agency. Orange square indicates Kashiwazaki-Kariwa Nuclear Power Station.

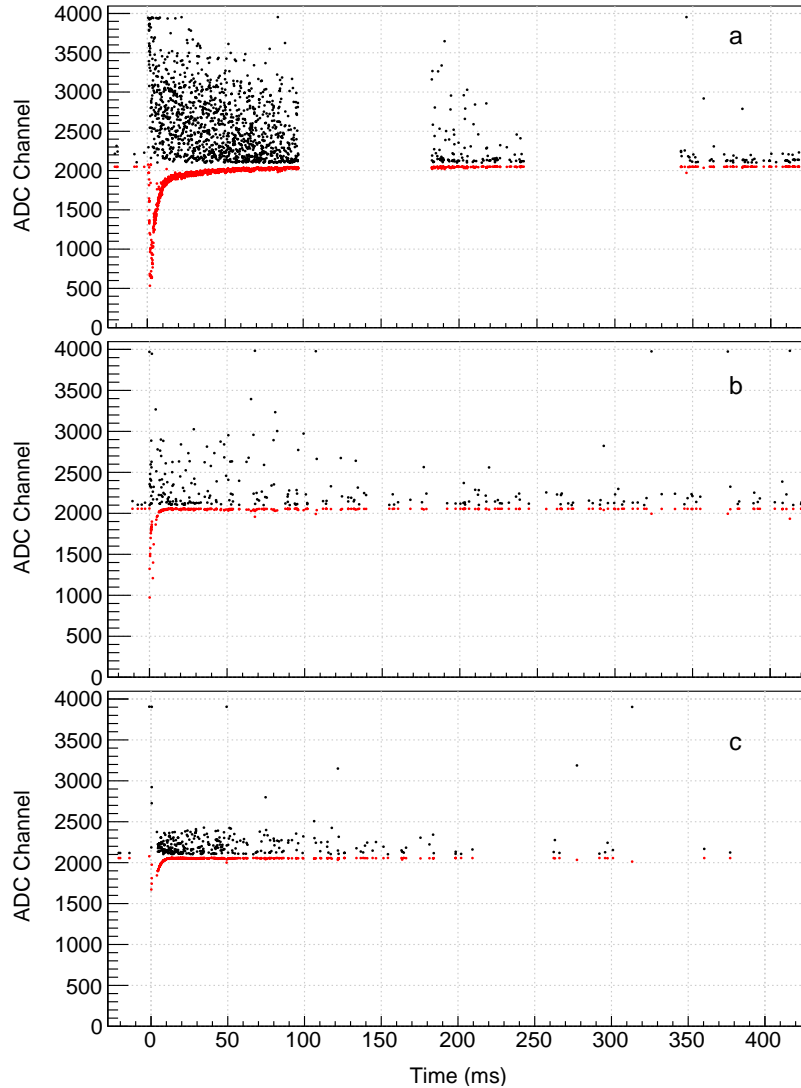


Figure 6: **Detector response to the initial radiation flash.** Panels **a–c** show the time histories of the (black dots) maximum and (red) minimum ADC values in the ADC-sampled waveforms of the detected photons with the detectors A, B, and C, respectively. Normally the minimum value is equal to the baseline (~ 0 V, at ADC = 2050 ch), but undershoot was observed in our experiments (see Methods). The energy 10 MeV corresponds to ADC increases of 1395, 1218, and 404 ch for the detectors A, B, and C, respectively.

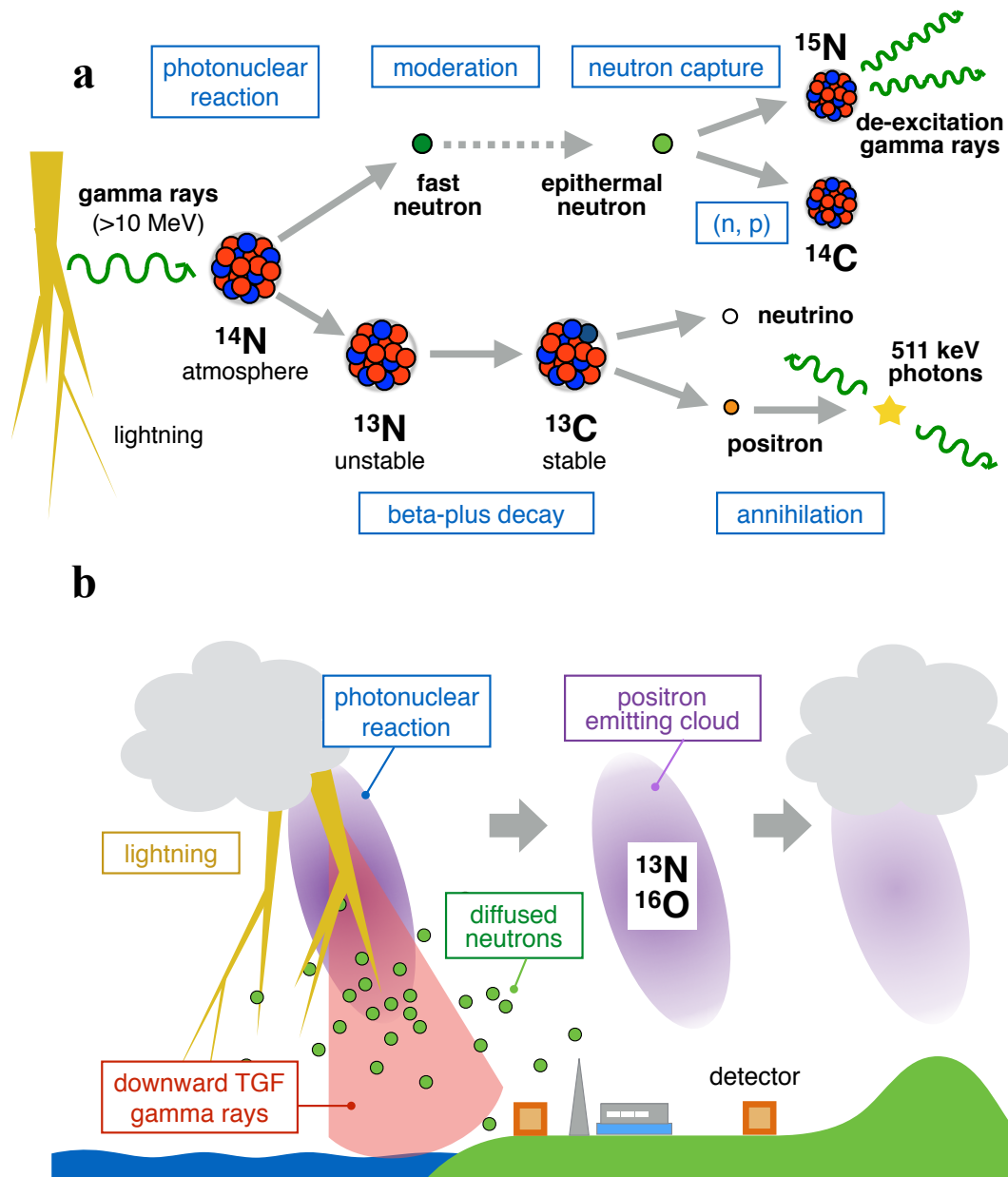


Figure 7: **Illustration of lightning-triggered physical processes.** **a**, Physical processes during a chain of the radiation events induced by the photonuclear reactions. **b**, Diffusion of neutrons produced in lightning, and drift of the positron-emitting cloud.

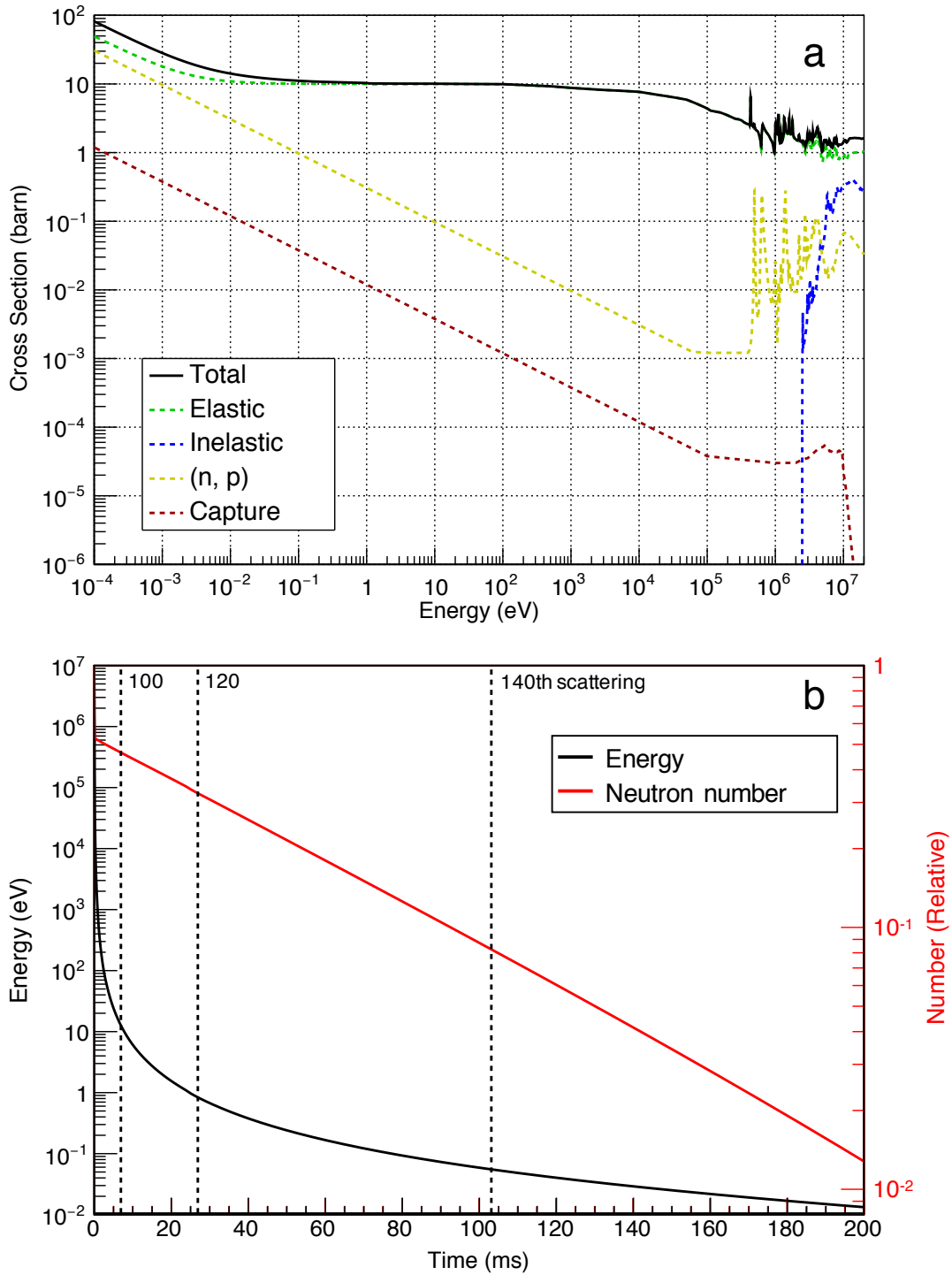


Figure 8: **Neutron cross-section on nitrogen and time profile of scattered neutrons.** **a**, (Black, curved) Neutron cross section on ^{14}N as a function of neutron kinetic energy ^{32,33}, including both (green) elastic and (blue) inelastic scatterings, (yellow) charged-particle production (n, p), and (red) neutron capture. **b**, (Black, curved) Kinetic energy and (red) relative number of neutrons as a function of time. The initial energy of neutrons is assumed to be 10 MeV, and the initial number of neutrons is normalised to 1. Dashed lines indicate the times for n -th scattering.

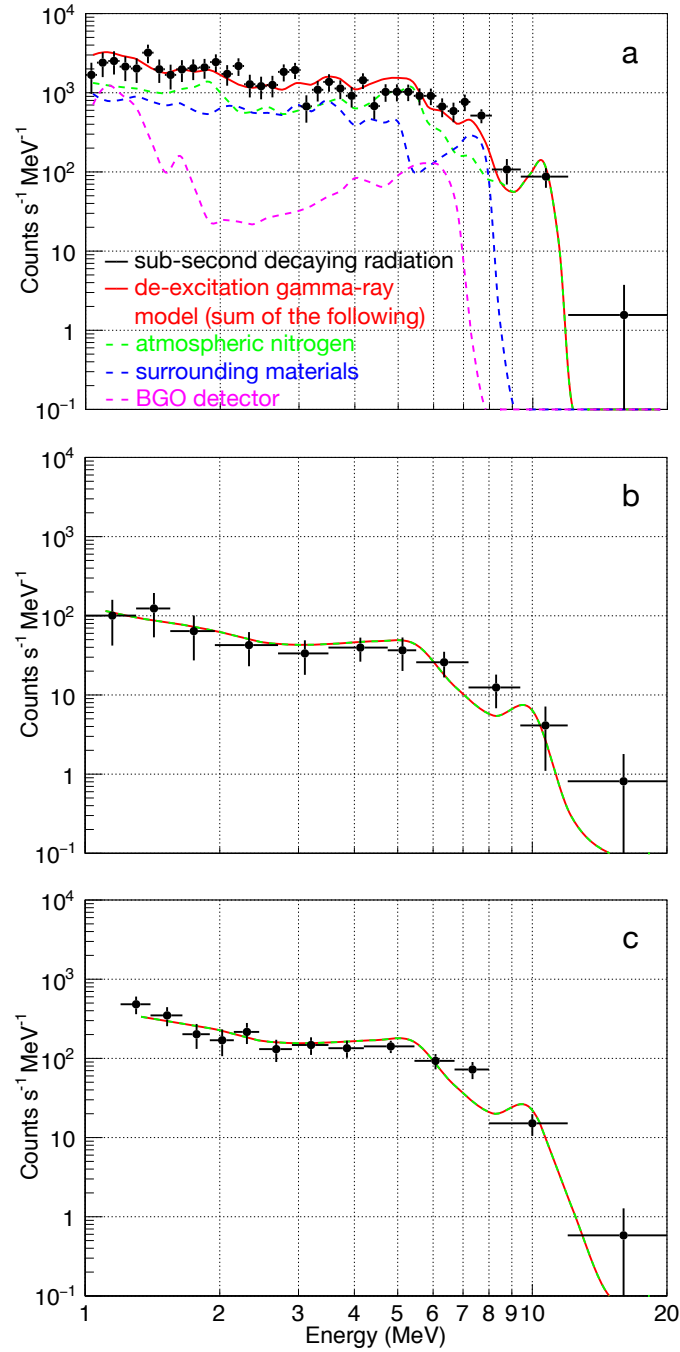


Figure 9: **De-excitation gamma-ray spectra compared with simulations.** Panels a–c show the background-subtracted gamma-ray spectra of the sub-second radiation with black crosses for $\pm 1\sigma$ errors in the detectors A, B, and C, respectively. The source events are extracted for the periods of $t = 40\text{--}100$ ms and $t = 20\text{--}200$ ms for the detectors A and B–C, respectively. The curves show the Monte Carlo simulations of de-excitation gamma rays from (green dashed-line) atmospheric nitrogen, (blue dashed) surrounding materials, (magenta dashed) detector itself, (red solid) and their total. The simulated spectra are normalised by the total counts above 1 MeV.

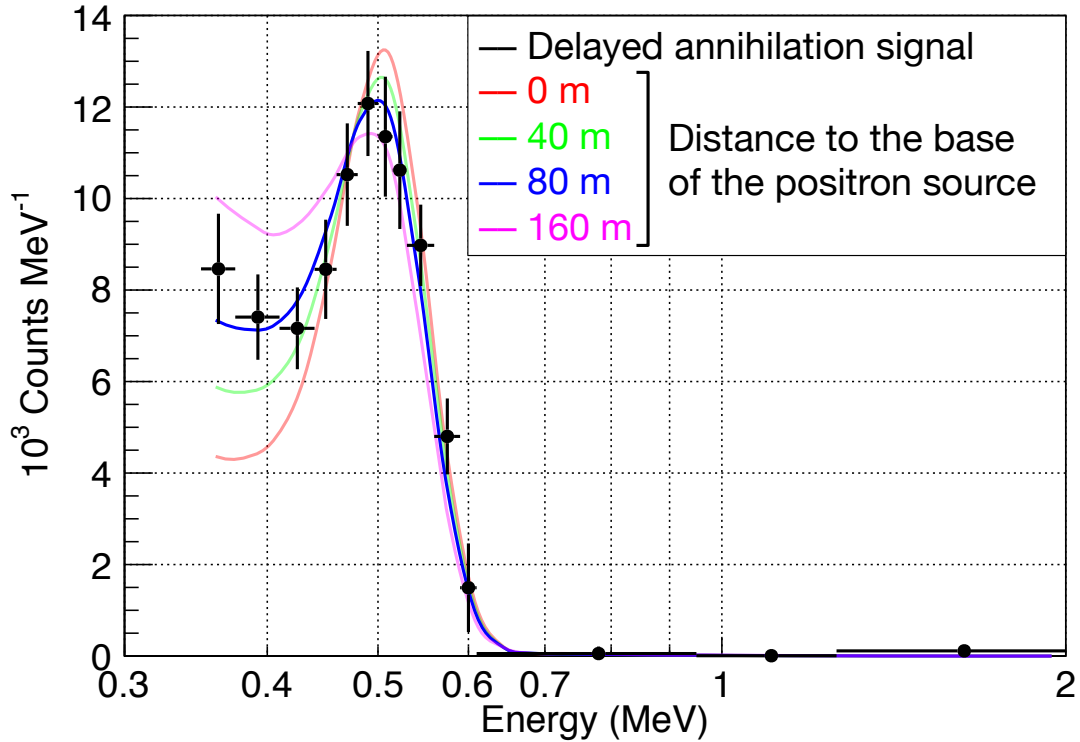


Figure 10: **Observed annihilation spectrum and simulated models.** The background-subtracted spectrum in the delayed phase with the detector A, accumulated over $t = 11.1\text{--}62.8$ s, is plotted with black crosses for $\pm 1\sigma$. The simulated model curves are overlaid for the assumed distances to the base of the positron-emitting cloud of (red) 0 m (*i.e.*, the detector is within the cloud), (green) 40 m, (blue) 80 m, and (magenta) 160 m. The models are normalised by the total counts in the 0.4–0.6 MeV band.

Table 1: Specifications and obtained values of our detectors (The error bars are in $\pm 1\sigma$).

Detector	A	B	C	D
Longitude	138.5960° E	138.6058° E	138.6014° E	138.5907° E
Latitude	37.4211° N	37.4222° N	37.4267° N	37.4200° N
Scintillation crystal	Cuboid BGO	Cuboid BGO	Cuboid BGO	Cylindrical NaI
Size (cm)	25 × 8 × 2.5	25 × 8 × 2.5	25 × 8 × 2.5	7.62 × ϕ 7.62
PMT type	2 × R1924A	2 × R1924A	2 × R1924A	R6231
Energy range (MeV)	0.35–13.0	0.35–13.0	1.2–48.0	0.2–27.0
Initial radiation flash				
Saturated dead time (ms)	< 40	< 20	< 20	< 300
Sub-second decaying radiation				
Decay constant (ms)	56 ± 3	55 ± 12	36 ± 4	saturated
Detected counts (20–220 ms)	1530	132	177	863
Energy range (MeV)	> 0.35	> 0.35	> 1.20	> 0.20
Prolonged annihilation signal (0.511 MeV line)				
Photon counts (Delayed comp.)	1830 ± 240 (1360 ± 210)	< 30 (1σ) –	out of range –	366 ± 50 –
Line centre (MeV)	0.515 ± 0.008	–	–	0.501 ± 0.007
Effective area (cm ²) at 0.511 MeV	149.2	149.2	out of range	28.3